

# A Climatology Based on Reanalysis of Baroclinic Developmental Regions in the Extratropical Northern Hemisphere

Laura de la Torre,<sup>a,b</sup> Raquel Nieto,<sup>a,c</sup> Marta Noguerol,<sup>a</sup>  
Juan Antonio Añel,<sup>a,b</sup> and Luis Gimeno<sup>a</sup>

<sup>a</sup>*Facultade de Ciencias de Ourense, Universidade de Vigo, Ourense, Spain*

<sup>b</sup>*Centre for Environmental and Marine Studies, Universidade de Aveiro, Aveiro, Portugal*

<sup>c</sup>*University of Lisbon, CGUL-IDL, Lisbon, Portugal*

Regions of the occurrence of different phenomena related to the development of baroclinic disturbances are reviewed for the Northern Hemisphere extratropics, using National Centers for Environmental Prediction/National Center for Atmospheric Research reanalysis data. The occurrence of height lows appears to be related to the orography near the earth's surface and with surface- and upper-air cyclogenesis in the upper troposphere. Over the cyclone tracks, the surface maxima appear to be trapped by land masses, whereas over the Mediterranean Sea they are located on the lee side of mountain ranges. The forcing terms of the geopotential tendency and omega equations mark the genesis (and, by the vorticity advection terms, the path) of the extratropical cyclones on the storm track. They occur mostly over the western coast of the oceans, beginning and having maxima on the lee side of the Rocky Mountains and the Tibetan Plateau. Their associated fronts form from the cold air coming from the continents and converging with the warm air over the Gulf and Kuroshio currents. Evident trends are found only for the Atlantic cyclone track (positive) and the Pacific cyclone track (negative) until the last decade when the tendency reverses. Over the southern Pacific, the number of fronts is lower during 1978–1997, coinciding with a period of strong El Niño Southern Oscillation episodes. This information is important for validating numerical models in order to predict changes associated with climate change and to study the behavior of extratropical cyclones and fronts.

*Key words:* baroclinic development; fronts; omega equation; geopotential tendency equation

## Introduction

Most synoptic-scale weather systems in mid-latitude regions appear to develop as a result of instability in the jet stream flow. This so-called “baroclinic” instability depends on the meridional temperature gradient, particularly at the earth's surface. The resulting differences in air density imply the existence of available potential energy that can be converted into kinetic

energy, above all in winter, from the increase in the pole-to-equator temperature gradient. A baroclinic disturbance develops, which may itself act to increase the pre-existing temperature gradient, thereby generating frontal zones.

These weather systems are most significant in the extratropics during winter, being responsible for clouds, precipitation, strong winds, and temperature changes. In extreme cases, they can lead to serious damage to infrastructure, through floods, hurricane-like winds, and severe storms. They can also affect transport links, leading to the isolation of rural communities and even deaths. They are also crucial

Address for correspondence: Laura de la Torre, Facultade de Ciencias de Ourense As Lagoas s/n, 32004-Ourense, Spain. ltr@uvigo.es

components of the earth's climate system because they regulate the contrast in temperature between the poles and the equator, stabilizing the stratification of air density and maintaining westerly winds in mid-latitude regions against frictional dissipation.

The most significant weather patterns that result from the development of baroclinic disturbances are extratropical cyclones, which are also associated with the generation of fronts. These cyclones originate in regions of pronounced horizontal temperature gradients that are located in the vicinity of the extratropical jet streams, and, occasionally, this temperature gradient is concentrated in a narrow frontal zone near the earth's surface. The nascent cyclone appears as a region of low pressure downwind (following the upper-level winds) of a pre-existing upper-level disturbance called a short-wave trough. As the cyclone continues to deepen, the upper-level disturbance intensifies, warm air advances poleward, and cold air advances toward the equator. The leading edges of these advancing air masses mark the location of the warm and cold fronts, respectively, near the earth's surface. When the cold air advances toward the equator, it causes the warmer air in lower latitudes to ascend, which generates a narrow zone of clouds and strong precipitation associated with the cold front. When the warm air advances poleward, it must ascend over the colder air found at the higher latitudes, and an extended region of clouds and moderate precipitation forms in front of this warm front. Eventually, the cyclone separates from the surface warm front and migrates toward the cold air, thus forming an occluded front. The deepening rate of the cyclone slows during this time and eventually ceases.<sup>1</sup>

The behavior of baroclinic systems depends on larger scale climate effects, such as the North Atlantic Oscillation (NAO) and the El Niño Southern Oscillation (ENSO). The NAO is a "see-saw" of atmospheric pressure between the Azores high and the Icelandic low that influences the path of extratropical cyclones over the Atlantic basin. When the NAO is positive,

both pressure centers deepen and this path displaces to the north.<sup>2</sup> The ENSO is a coupled atmosphere–ocean variability effect that is located over the tropical South Pacific. When an ENSO event occurs, the sea surface temperature pattern and the pressure pattern change over this region, modifying the circulation at low and high levels and thus displacing the jet streams. These events, therefore, produce pressure, temperature, and precipitation anomalies all over the globe.<sup>3</sup>

### Regions of Occurrence of Extratropical Cyclones

The distribution of extratropical cyclones is far from homogeneous. These cyclones form preferentially in some mid-latitude regions, called storm tracks. Following Sickmüller *et al.*,<sup>4</sup> we will distinguish between "storm track" and "cyclone track." A storm track is defined as a region that has an increased standard deviation of variability with respect to the band-pass, filtered (2.5–6 days), 500 hPa, geopotential height.<sup>4,5</sup> This definition means that the storm track takes variability into account that is unrelated to geopotential height minima (see Ref. 6). A cyclone track, on the other hand, is a region of increased density of synoptic cyclones and thus is only related to geopotential height minima. Most existing cyclone climatologies use algorithms that can be categorized into nontracking and tracking techniques. The former regard cyclones as single points in space that are represented by their center (e.g., the location of the minimum sea level pressure) and yield climatological cyclone center density fields (e.g., Refs. 7, 8). Although this approach is reasonably straightforward, it cannot provide information about the genesis and lysis of cyclones. Most existing climatologies fall into the second category and are based on some kind of cyclone-tracking technique.<sup>4,9</sup>

In the Northern Hemisphere, major storm/cyclone tracks extend from the east coast of the continents northeastward across the oceans. In the North Atlantic, systems either

turn northward into Baffin Bay or, more frequently, continue northeastward to Iceland and the Norwegian Barents Sea. In the North Pacific, systems move from eastern Asia toward the Gulf of Alaska. Cyclones form, or are re-developed, east of the Rocky Mountains in Alberta and Colorado and move eastward toward the Great Lakes and Newfoundland before turning northward toward Greenland and Iceland.<sup>10</sup> The spatial distribution of systems identified by Serreze *et al.*<sup>11</sup> shows that in winter months the cyclone maximum near Iceland extends northeastward into the Norwegian Barents Sea. In winter, both the rate of cyclone deepening and the frequency of deepening events peak in the area of the Icelandic low, southwest of Iceland, with a separate maximum in the Norwegian Sea.<sup>12</sup> These locations show a high frequency of cyclogenesis, cyclone filling, and cyclolysis, which implies that this sector of the Arctic is dynamically active with alternating regimes. Gyakum *et al.*<sup>13</sup> found that in the Pacific Ocean, although the greatest cyclone frequency is located between lat 50°N and 65°N in the Gulf of Alaska and in the vicinity of the Kamchatka Peninsula, the highest percentage of deepening cyclones exists in areas south of lat 50°N. These authors also found that over 90% of cyclones that pass through the region of the Kuroshio Current intensify. This percentage gradually diminishes to the east. In fact, systems forming over the oceans intensify over strong gradients of sea surface temperature. Over the Mediterranean Sea, Trigo *et al.*<sup>14</sup> found strong cyclogenesis maxima over the Gulf of Genoa, south of the Atlas Mountains and in the Middle East.

Cyclone tracks vary over time, but the precise nature of their variability remains to be mapped. The interpretation of the results obtained depends on the tracking algorithm used and on the conditions that are imposed, such as cyclone intensity or duration.<sup>4</sup> Hence, such results as have been obtained sometimes seem to contradict each other. Lambert<sup>15</sup> observed an increase in the number of intense cyclones in the Northern Hemisphere after

1970. Schinke<sup>16</sup> found a similar result over Europe and the North Atlantic. Key and Chan<sup>17</sup> showed that, in winter, closed lows increase in frequency in the range lat 60–90°N and decrease in the range lat 30–60°N. They also found a relationship between the geopotential tendency in the Arctic and the NAO. Sickmüller *et al.*<sup>4</sup> observed an increase in cyclone density and storm track in the Atlantic basin, but they reported the opposite trend in the Pacific basin. Graham and Diaz<sup>18</sup> found an increase in cyclone intensity over time in the Pacific. Chen *et al.*<sup>19</sup> found a decrease in the frequency of cyclogenesis over east Asia, which ceases after 1977.

### Identification of Fronts

The concept of atmospheric fronts was introduced by the Bergen school early in the 20th century.<sup>20</sup> Fronts are associated with gradients of temperature, dew point, wind velocity, barometric tendency, and vertical motion of air masses. Since this pioneering work, considerable advances have been made in computing and observational technology. Despite these advances, however, there is still no widely accepted objective method of recognizing atmospheric fronts. Recognition depends on two factors: (i) the definition of a front and (ii) methods for determining whether or not the criteria specified in the definition have been met. For a complete description of the different definitions and criteria used by other authors, see Ref. 21. Even when using subjective methods, different forecasters will frequently produce different analyses of the presence of fronts on the basis of the same data sets.<sup>22</sup>

The first publication concerned with the objective identification of fronts was by Renard and Clarke.<sup>23</sup> Their pioneering methodology for the objective identification and location of fronts in gridded data sets is based on the primary (thermal) definition, according to which an atmospheric front is defined as the “warm air boundary of a synoptic scale baroclinic zone of distinct thermal gradient.” They defined

a variable called the *Thermal Front Parameter* (TFP), which represents the gradient of the magnitude of the thermal gradient, resolved parallel to its direction. This methodology has been used by many subsequent authors (for example, Refs. 24–26) and is the one used in this work. Renard and Clarke<sup>23</sup> used the potential temperature to compute the TFP. However, atmospheric motion around fronts is generally not dry adiabatic. The main alternative is thus to use a variable such as wet bulb potential temperature or equivalent potential temperature, which are essentially conserved during moist ascent and descent and hence act as better tracers of air mass. One of the more recently proposed methods for the objective identification and plotting of fronts, which uses its precise dynamic definition, is documented by Hewson.<sup>21</sup> Both objective and subjective techniques for locating fronts have been widely used in weather analysis and forecasting and for studying the characteristics of fronts using case studies (see Refs. 27–29).

It has been shown that:

$$TFP = -\vec{\nabla}|\vec{\nabla}\theta_e| \cdot \frac{\vec{\nabla}\theta_e}{|\vec{\nabla}\theta_e|} \text{ (see Ref. 21)} \quad (1)$$

where  $\theta_e = [T + q \cdot \frac{L}{C_p}] \cdot [\frac{P_0}{P}]^{\frac{R}{C_p}}$  (see Ref. 30), where  $T$  is temperature,  $q$  is specific humidity,  $L$  is the vaporization latent heat,  $C_p$  is the specific heat of dry air at constant pressure,  $P$  is pressure,  $P_0$  is pressure at a standard level (1000 hPa),  $R$  is the gas constant for dry air, and  $\theta_e$  is the equivalent potential temperature.

The first factor in the TFP equation describes the change in the temperature gradient; the second factor describes the projection of the first term resolved in the direction of the temperature gradient. There is a clear relationship between the TFP as a frontal analysis parameter and the well-known basic definition of a front, which fixes a cold front where temperature begins to fall and a warm front where the rise of temperature ends. This definition is identical to the definition of the maximum of the TFP.

### Dynamics of Baroclinic Development: The Quasigeostrophic Approximation

The idea that development of baroclinic disturbances occurs almost in geostrophic and hydrostatic balance has led to the adoption of quasigeostrophic dynamics in its study, which in turn represents a simplification of the governing equations. Quasigeostrophic theory still provides the primary conceptual model used by synoptic meteorologists for understanding weather patterns, as well as for evaluating the performance of numerical models used in forecasting. This theory is often summarized in the application of the geopotential tendency and omega equations (e.g., Refs. 10, 31). The usual forms of both these equations contain two primary forcing terms, which are not independent and thus lead to difficulties in physical interpretation, but they nevertheless have separate physical meanings. This approximation assumes that the effects of diabatic heating, surface friction, and orography are negligible.

The omega equation [Equation (2)] expresses the synoptic scale vertical motion [represented by the three-dimensional Laplacian of omega (term A)] as the sum of the advection of absolute geostrophic vorticity in the geostrophic wind (term B) and the Laplacian of the temperature (term C).

$$\underbrace{\left( \nabla^2 + \frac{f_0^2}{\sigma} \frac{\partial^2}{\partial P^2} \right) \omega}_{A} = \underbrace{\frac{f_0}{\sigma} \frac{\partial}{\partial P} [V_g \cdot \nabla(\xi_g + f)]}_{B} + \underbrace{\frac{1}{\sigma} \nabla^2 \left[ V_g \cdot \nabla \left( -\frac{\partial \phi}{\partial P} \right) \right]}_C \text{ (see Ref. 31)} \quad (2)$$

where  $\omega$  is the vertical component of the wind velocity when pressure is used as the vertical coordinate, where  $f$  is the Coriolis parameter,  $f_0$  is the Coriolis parameter at a reference latitude,  $\sigma$  is the standard atmosphere static stability parameter in isobaric coordinates,  $V_g$  is the geostrophic wind,  $\xi_g$  is the geostrophic relative vorticity,  $\phi$  is the geopotential.

Term A is proportional to the upward motion but opposite in sign (see Ref. 32). Term

B represents the vertical variation of absolute vorticity advection. At the synoptic scale, only relative vorticity advection needs to be taken into account. Where cyclonic vorticity advection increases with altitude, the upward motion is favored, as is the case in the Northern Hemisphere. Term C involves the Laplacian of the thickness advection. The existence of a maximum thickness advection implies that warm air forces upward motion. Although terms B and C often largely cancel each other out, they may nevertheless be clearly interpreted as separate physical processes.

The geopotential tendency equation provides a relationship between the local geopotential tendency (term A) and the distributions of vorticity advection (term B) and thickness advection (term C).

$$\underbrace{\left[ \nabla^2 + \frac{\partial}{\partial P} \left( \frac{f_0^2}{\sigma} \frac{\partial}{\partial P} \right) \right]}_A \chi = \underbrace{-f_0 \dot{V}_g \cdot \nabla (\xi_g + f)}_B - \underbrace{\frac{\partial}{\partial P} \left[ \frac{-f_0^2}{\sigma} \dot{V}_g \cdot \nabla \left( -\frac{\partial \phi}{\partial P} \right) \right]}_C \quad (3)$$

where  $\chi = \frac{\partial \phi}{\partial t}$  and  $\sigma = -\frac{RT_0}{P} \frac{d \ln \theta_0}{dP}$  (see Ref. 31),  $t$  is time,  $T_0$  is temperature in a basic state, and  $\theta_0$  is the potential temperature corresponding to  $T_0$ .

Term A involves second derivatives in space of the geopotential tendency field and is thus generally proportional to the tendency, but opposite in sign. Term B is proportional to the advection of absolute vorticity. At short wavelength and at synoptic scale (horizontal scale  $<3000$  km), only relative vorticity advection needs to be taken into account. This equation implies that positive relative vorticity advection is related to falling geopotential heights. This term acts to propagate the disturbance horizontally and to spread it vertically. The major mechanism for the amplification or decay of mid-latitude synoptic systems is contained in term C. This term involves the vertical variation of the horizontal thickness advection, and it acts to enhance upper-level

height anomalies in developing disturbances. When the thickness advection increases with altitude, it acts to intensify the troughs in the upper troposphere. Given that it is related to differential temperature advection with height, this term implies that mid-latitude synoptic systems are intensified through baroclinic processes.

## Objectives

In the study reported herein, the regions of occurrence of these baroclinic phenomena were investigated with respect to their location and characteristics. Given that cyclogenesis and lysis were not of primary interest, a simple non-tracking algorithm was used to detect lows not only near the earth surface but also in the middle and upper troposphere. The locations of the fronts were identified by means of the TFP, as defined by Renard and Clarke,<sup>23</sup> and using the equivalent potential temperature method to determine their more approximate position. The forcing terms of the omega and geopotential tendency equations were determined in order to obtain the dynamic characteristics of the fronts. As far as we know, this is the first time that the climatology of these forcing terms and fronts has been studied. Their regions of occurrence are related to lows and storm tracks.

## Data and Methods

Data for the geopotential height, humidity, wind, and temperature at 12:00 UTC for the period December 1957–February 2006 were obtained using a National Center for Environmental Prediction/National Center for Atmospheric Research (NCEP/NCAR) re-analysis technique.<sup>33</sup> The spatial resolution in longitude and latitude was  $2.5^\circ$ . As baroclinic development is more important during winter, only data for December, January, and February were included in our analysis. Thus for example, using this convention, winter 1958 is represented by the months of December 1957,

January 1958, and February 1958. The region under investigation covers all longitudes from 20°N to 70°N, thus embracing the more important areas of baroclinic development in the Northern Hemisphere. Three vertical levels were used (850 hPa, 500 hPa and 200 hPa), representing the three different parts of the troposphere under discussion (near-surface troposphere, middle troposphere, and high troposphere, respectively).

In this way, we aimed to identify:

- minima of geopotential height at 850 hPa, 500 hPa, and 200 hPa in order to find deep troughs and lows. When the geopotential height at a central point was lower than six or more of the surrounding eight points, it was considered a minimum of geopotential height. This criterion applied not only for closed lows but also for deep troughs related to baroclinic development. Then, we counted the times each grid point fulfilled the condition of minima.
- high positive values of TFP at 850 hPa to find surface fronts, using Equation (1). We counted the times TFP was higher than  $2 \text{ K/m}^2$
- maxima (value at a central point is greater than at the surrounding eight points) of
  - a) vorticity advection ( $-V_g^1 \cdot \nabla \xi_g$ ) at 500 hPa;
  - b) thickness advection ( $-V_g \cdot \nabla(-\partial Z/\partial P)$ ), being  $Z$  the geopotential height), thickness considered between 200 hPa and 500 hPa;
  - c) differences between vorticity advection at 200 hPa minus vorticity advection at 850 hPa;
  - d) differences between thickness advection at 200–500 hPa minus thickness advection at 500–850 hPa

in order to find regions of upward movement of air masses or regions with a negative geopotential tendency. Then, we counted the times each grid point fulfilled the condition of maxima.

In order to characterize the climatology, we tested several thresholds in an attempt to identify only those points that are related specifically to baroclinic development and to thus filter out noise. We then added in all the data points that satisfied the threshold condition during the period. In order to investigate the variability, we further subdivided the whole period into approximately 10-year intervals (1958–1967, 1968–1977, 1978–1987, 1988–1997, and 1998–2006) and carried out computations for each interval, taking into account the number of years (generally 10 apart from the final interval, which was nine).

## Results

### Detection of Deep Troughs and Lows: Geopotential Height Minima

Figure 1 shows the distribution of winter geopotential height minima for the period 1958–2006 at 200, 500, and 850 hPa. Atlantic and Pacific cyclone tracks appear at the three levels, with a low-level pattern similar to the one found by Wernli and Schwierz.<sup>9</sup> The Atlantic cyclone track extends from Hudson Bay to the northern coast of Europe and has two local maxima. The maximum between Greenland and Iceland is the stronger one, but its intensity decreases with height. The maximum over Hudson Bay, in contrast, maintains its intensity throughout the troposphere. The Pacific cyclone track extends from the east coast of Asia to the west coast of America and is confined to lat 40–60°N. There are two local maxima, one over the Gulf of Alaska that diminishes with height and another one west of Kamchatka that does not. These centers were reported previously by Gyakum *et al.*<sup>13</sup> using surface charts. These cyclone tracks are just north of the storm tracks, defined as the root mean square of the band-pass filtered 500 hPa geopotential height (see Ref. 4 for an example of this).

Apart from the cyclone tracks, there is another important region of occurrence of

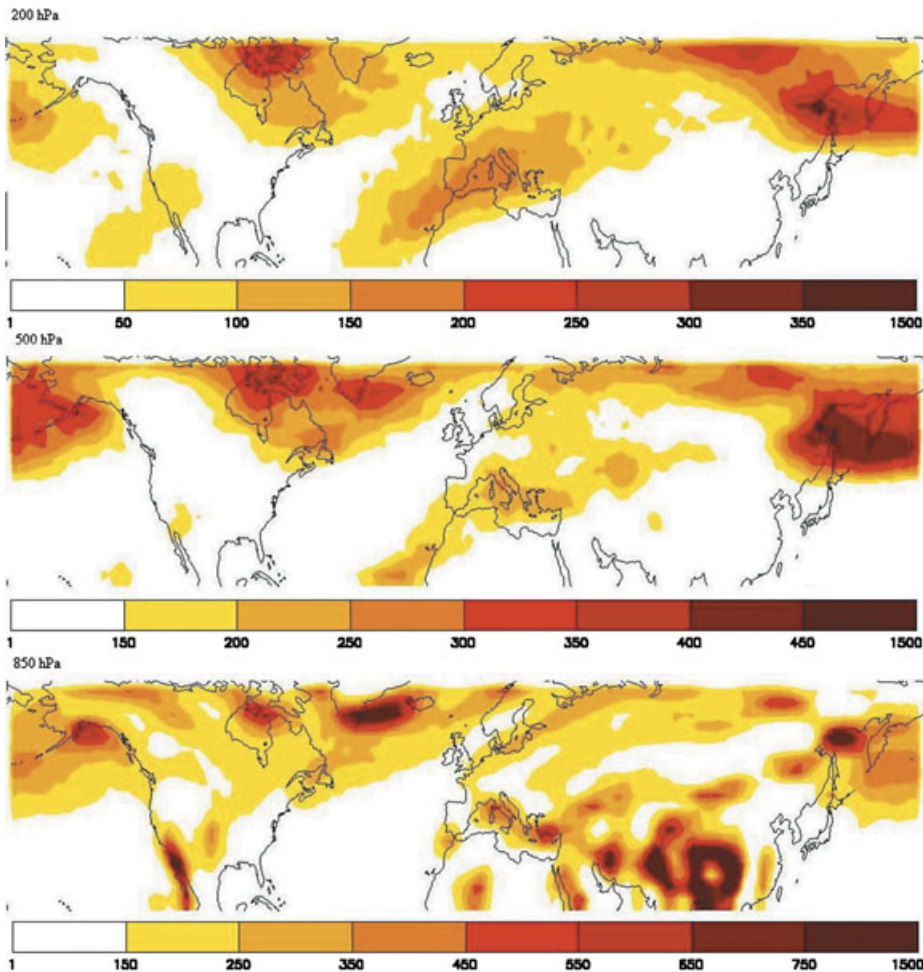


**Figure 1.** Total number of geopotential height minima by grid point for winters (December, January, and February) from 1958–2006 at three vertical levels: 200 hPa (first row), 500 hPa (second row), and 850 hPa (third row).

extratropical cyclones over the Mediterranean Sea.<sup>9,34</sup> Local maxima are found over the northern coast of the Mediterranean Sea (Fig. 1). These coincide with the cyclogenesis maxima found by Trigo *et al.*,<sup>14</sup> although in some cases with some displacement eastwards. These maxima are located over the Gulf of Genoa, south of the Atlas Mountains, east of the Aegean Sea, east of the Black Sea, and northeast of the Persian Gulf. We also find a maximum southwest of the Strait of Gibraltar and in the western part of the Arabian Peninsula. At higher levels, there is a maximum that extends from the western part of the Mediterranean Sea to the northwest of the Canary Islands, which resembles the

maximum of cut-off lows found by Nieto *et al.*<sup>35</sup> for the European sector.

Over Asia there is a maximum over northern Siberia that reaches 200 hPa and appears to merge with the Pacific cyclone track in the middle and high levels. This maximum was also observed by Chen *et al.*<sup>19</sup> using surface charts. The maxima found at 850 hPa over the Tibetan Plateau are probably related to the existence of the monsoon winter high and are not connected with any baroclinic development. The same reasoning can be applied to the maximum over Baja California (Mexico). Finally, there is some evidence of maxima on the lee side of the Himalayas but only in the 850 hPa surface.

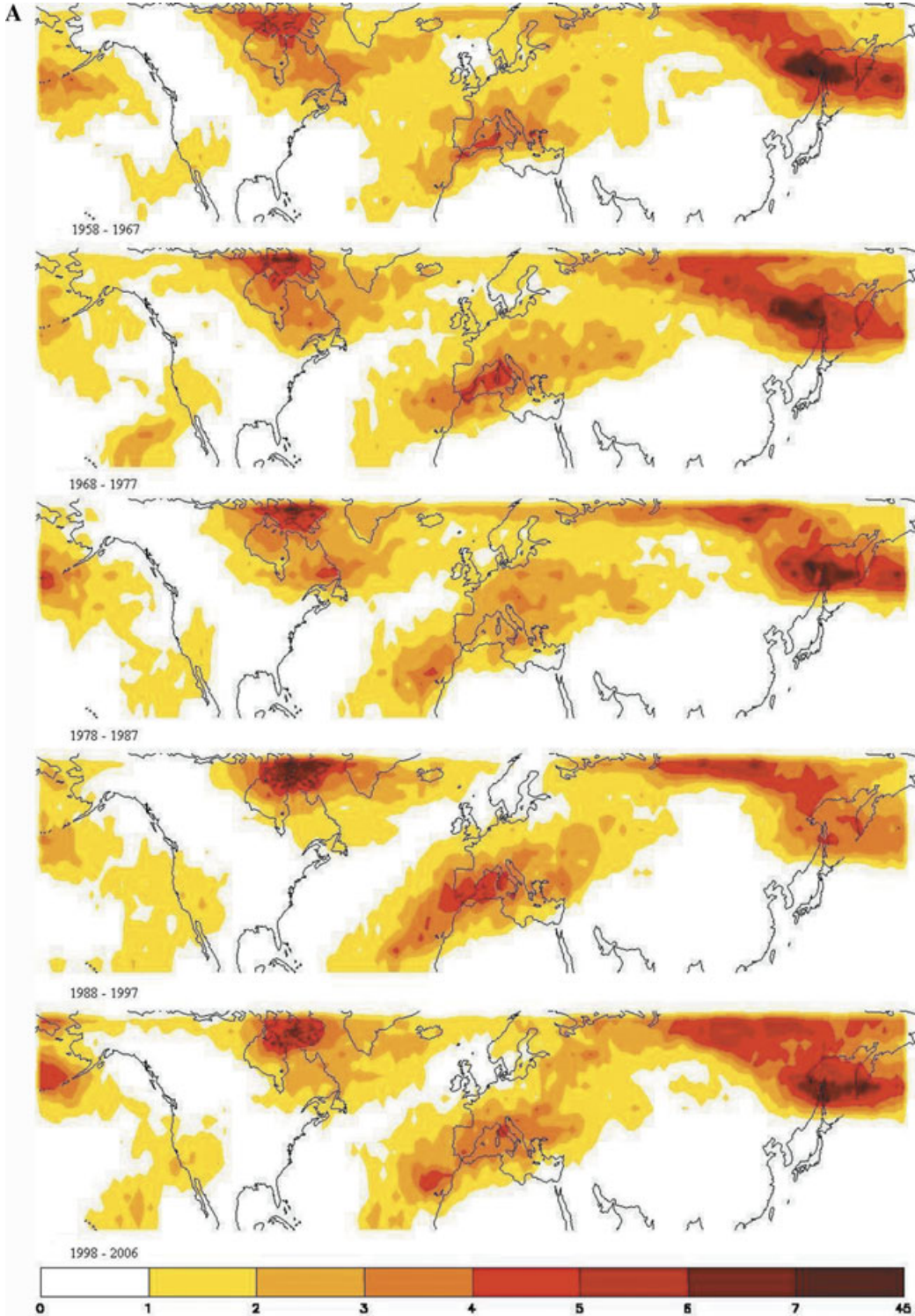


**Figure 2.** Total number of geopotential height minima by grid point and year for 1958–1967 (first row), 1968–1977 (second row), 1978–1987 (third row), 1988–1997 (fourth row), and 1998–2006 (fifth row). **A)** 200 hPa, **B)** 500 hPa, **C)** 850 hPa.

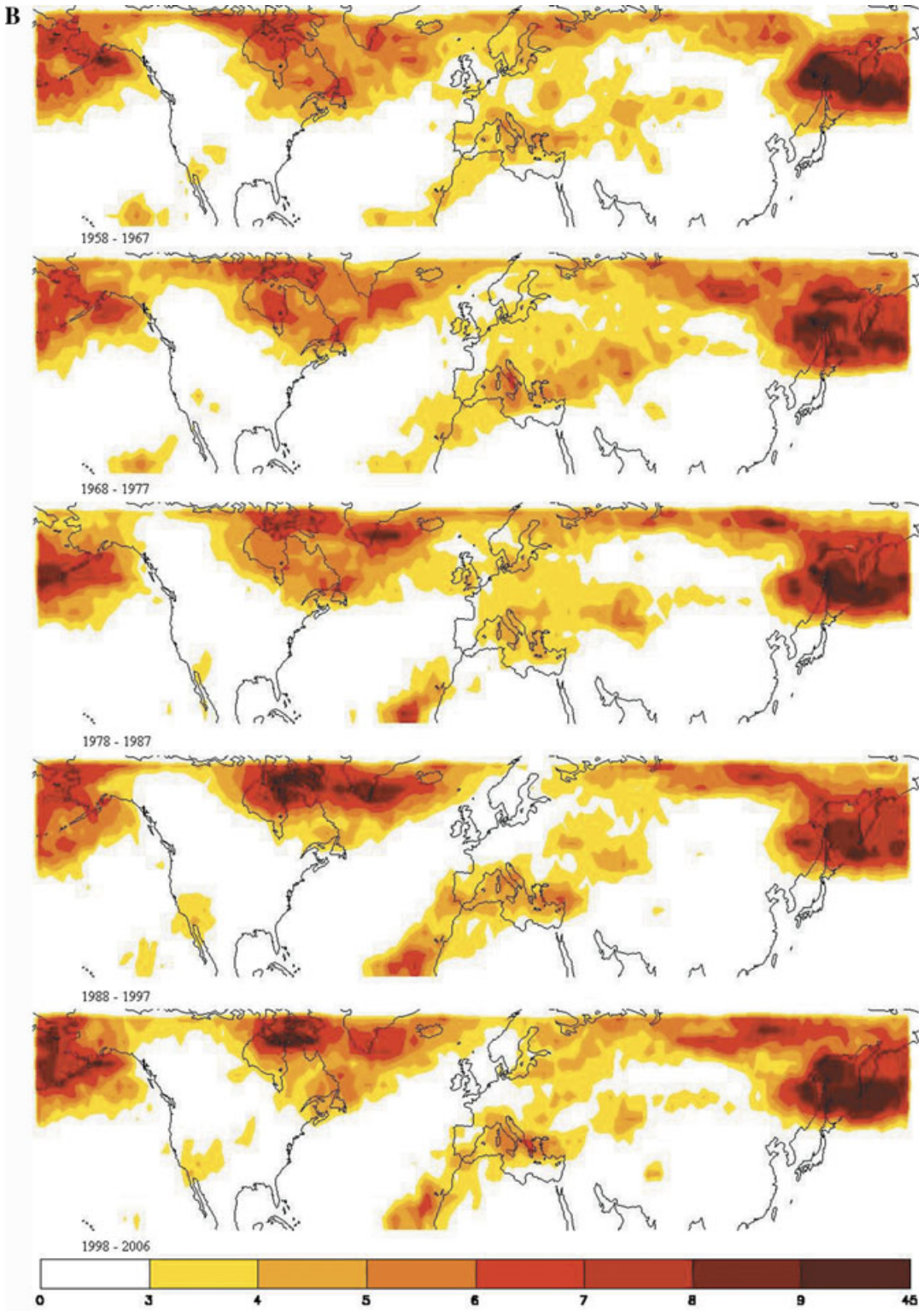


**Figure 2.** *Continued*

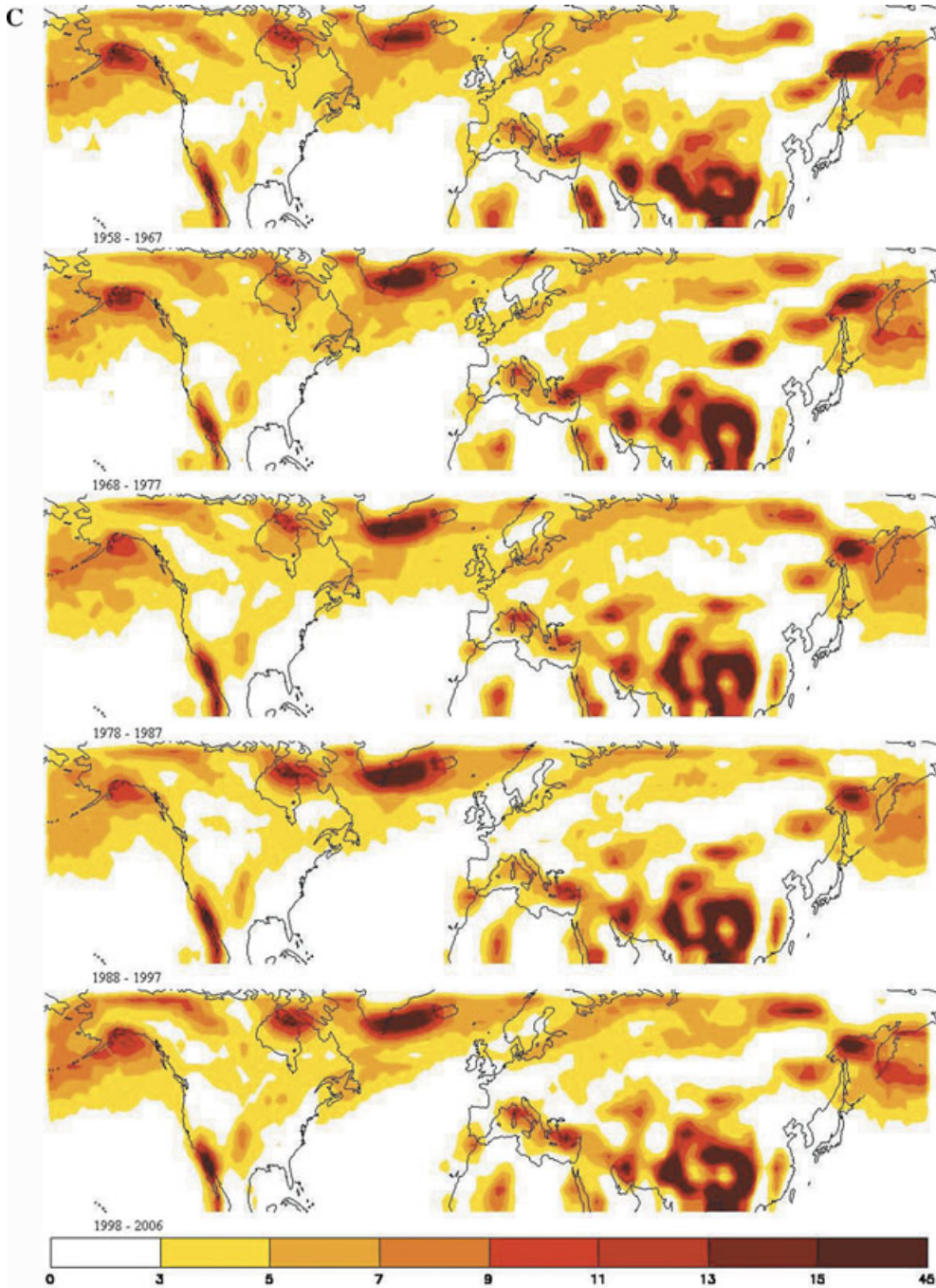


**Figure 2.** *Continued*

In order to better understand the variability in the occurrence of the geopotential height minima, Figure 2 shows the number of minima per year during the different 10-year periods at (A) 200 hPa, (B) 500 hPa, and (C) 850 hPa. In

the Atlantic cyclone track, there was an increase in the number of minima up to the 1990s, which has been related to the increase of the NAO index and the subsequent northward shift of the storm track.<sup>36</sup> In the last decade, there has

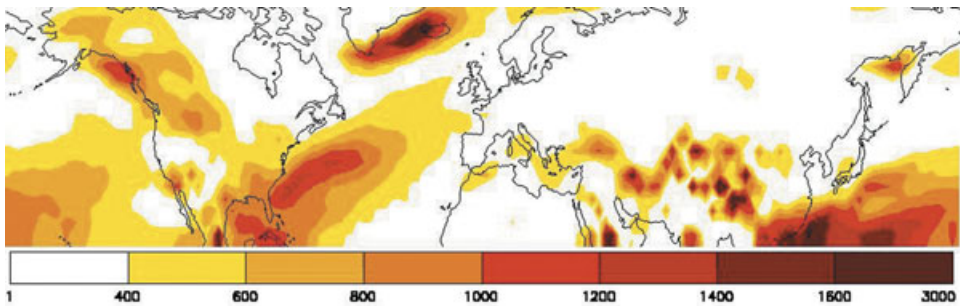


**Figure 3.** Total number of times the thermal frontal parameter is greater than  $2 \text{ K/m}^2$  by grid point for the winters (December, January, and February) from 1958–2006 at 850 hPa.

been a change in this tendency, with a strong decrease in the number of minima, which is also consistent with the decrease found in the NAO Index. The evolution of the Pacific cyclone track has shown the opposite behavior, with a decrease in the number of minima until the 1990s and an increase thereafter. This downward trend seems to contradict the upward trend found by other authors (e.g., Ref. 37) and is not consistent with the northward trend in the Pacific storm track.<sup>4</sup> Apart from the dependence of the results on the tracking algorithm, Sickmüller *et al.*<sup>4</sup> identified different trends, which depend on the duration, intensity, and geopotential height gradients of the cyclones. In their study, they found that in the Pacific there is a decrease in the number of cyclones with at least a 3-day lifetime, the geopotential height gradients are less intense, and there is a decrease in cyclones with very low central height. The maxima not related to the Atlantic or the Pacific cyclone tracks show a high variability over the 10-year intervals, with no trends evident.

### Detection of Fronts: The Thermal Front Parameter

The threshold taken for the TFP was  $2 \text{ K/m}^2$ , and this was verified using several examples of fronts appearing in satellite images. This TFP at 850 hPa gives an approximation of the location of developed surface fronts associated with extratropical cyclones.

Figures 3 and 4 show the climatology of these phenomena for the 49 winters under investigation and their variability over the 10-year intervals, respectively. Apart from the maxima associated with the Pacific and Atlantic cyclone tracks, west of Kamchatka and between Greenland and Iceland, there is a weak signal over the Mediterranean Sea and strong maxima where the cold westerlies coming from the continents converge with the humid and warm air over the Gulf and Kuroshio currents. In the Atlantic, the maximum extends from the Gulf of Mexico through the eastern border of the Gulf current to the west coast of Europe, whereas in the Pacific the maxima are confined to the lower latitudes where the water is warmer. They are located just south of the storm track. The barrier effect of the Rocky Mountains, which prevents the passage of the fronts from the west, is clear from these figures. The maximum over Asia is related to orographical forcing, which plays a role in the developing of a front. There is also a signal over the Arabian Peninsula east of the geopotential height minima found in Figure 1.

It may be seen in Figure 4 that the centers directly related to the cyclone tracks have a minimum number of fronts during the period 1978–1987, increasing thereafter. Over the Gulf Stream, the center is stronger during 1988–1997, with an evolution similar to that of the geopotential height center between Greenland and Iceland that can be related to the NAO. In the southern Pacific, the number

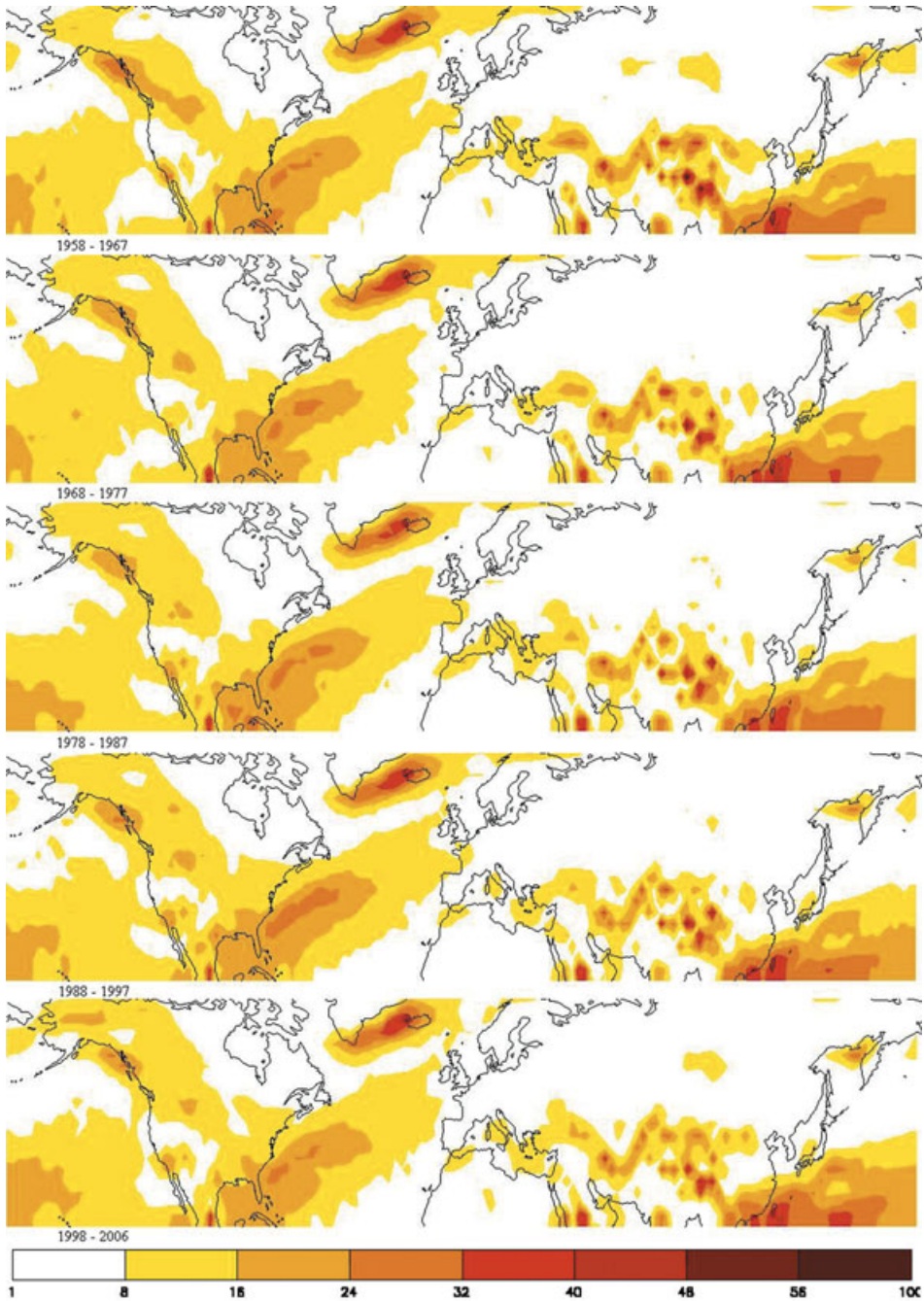


**Figure 4.** Total number of times the thermal frontal parameter at 850 hPa is greater than  $2 \text{ K/m}^2$  by grid point and year for 1958–1967 (first row), 1968–1977 (second row), 1978–1987 (third row), 1988–1997 (fourth row), and 1998–2006 (fifth row).

of fronts is lower during 1978–1997, coinciding with strong ENSO episodes, which implies positive anomalies of geopotential height over the region and negative anomalies of precipi-

tion, which are probably related to this lower number of fronts. Over the Mediterranean Sea there is strong variability over the whole period.

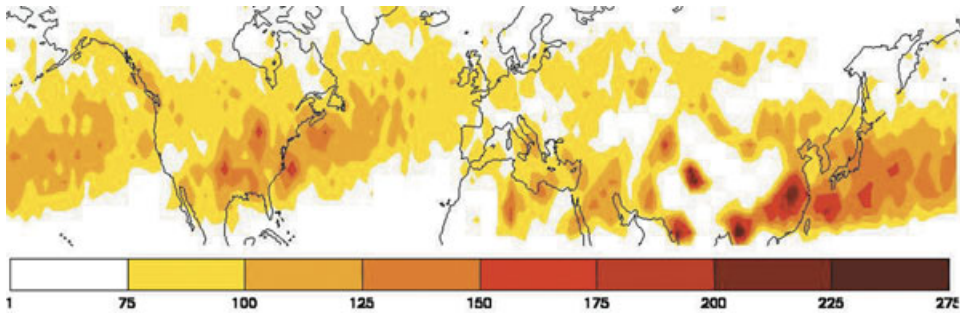


**Figure 5.** Total number of times the vorticity advection at 500 hPa is greater than  $6 \text{ s}^{-2}$  by grid point for 1958–2006 winters (December, January, and February).

### Detection of Regions Where the Geopotential Tends to Drop: The Geopotential Tendency Equation

The quasigeostrophic approximation provides a simple method for studying regions of potential decrease in geopotential or regions where the conditions favor the upward movement of air masses. The geopotential tendency equation yields information about changes in geopotential.

The equation has two forcing terms that have been studied separately. Term B, or the vorticity advection term, is represented in Figure 5 and is related to a drop in pressure from the movement of the cyclone systems. In this case, we have chosen a threshold of  $6 \text{ s}^{-2}$ . The regions where the pressure tends to drop from positive vorticity advection resemble the cyclogenesis regions identified by Wernli and Schwierz<sup>9</sup> south of lat  $50^\circ\text{N}$ . They seem to be related to the storm tracks and not to the cyclone tracks, which are perhaps related to stationary cyclones (in fact, the maxima in Figure 1 are located between land areas). There is a maximum over the eastern part of North America that extends through the Atlantic to Ireland and another maximum on the lee side of the Tibetan Plateau that extends through the Pacific to the west coast of North America. The association between these transient lows and the frontal regions found over the Gulf and Kuroshio currents is clear. There is also another maximum related to the cyclogenesis in

the Mediterranean Sea. Figure 6 shows that the 10-year variability is reflected in changes in the distribution within the centers and not in the intensity, except for the last period (1998–2006) when there is a general drop in the number of points that satisfy the criteria.

Term C is concentrated at the beginning of the Pacific and Atlantic storm tracks, just north of the term B maxima (Fig. 7), and also reaches a maximum over the Arabian Peninsula. This term represents the forcing from different temperature advection at higher and lower levels and is related to the strong intensification of the lows that occurs mostly during the first stages of their existence. The 10-year variability (Fig. 8) shows a redistribution of the maxima within the centers.

### Detection of Regions Where Upward Movements Are Favored: The Omega Equation

In order to identify those regions where the upward movement of air masses is favored, the climatologies of terms B and C of the omega equation are displayed in Figures 9 and 11, respectively. These regions generally coincide with the ones shown in Figures 5 and 7 (i.e., the terms of the geopotential tendency equation), although term C registers slightly in northern Eurasia and eastern Greenland. Thus, the regions where pressure tends to drop are the regions where these upward movements are

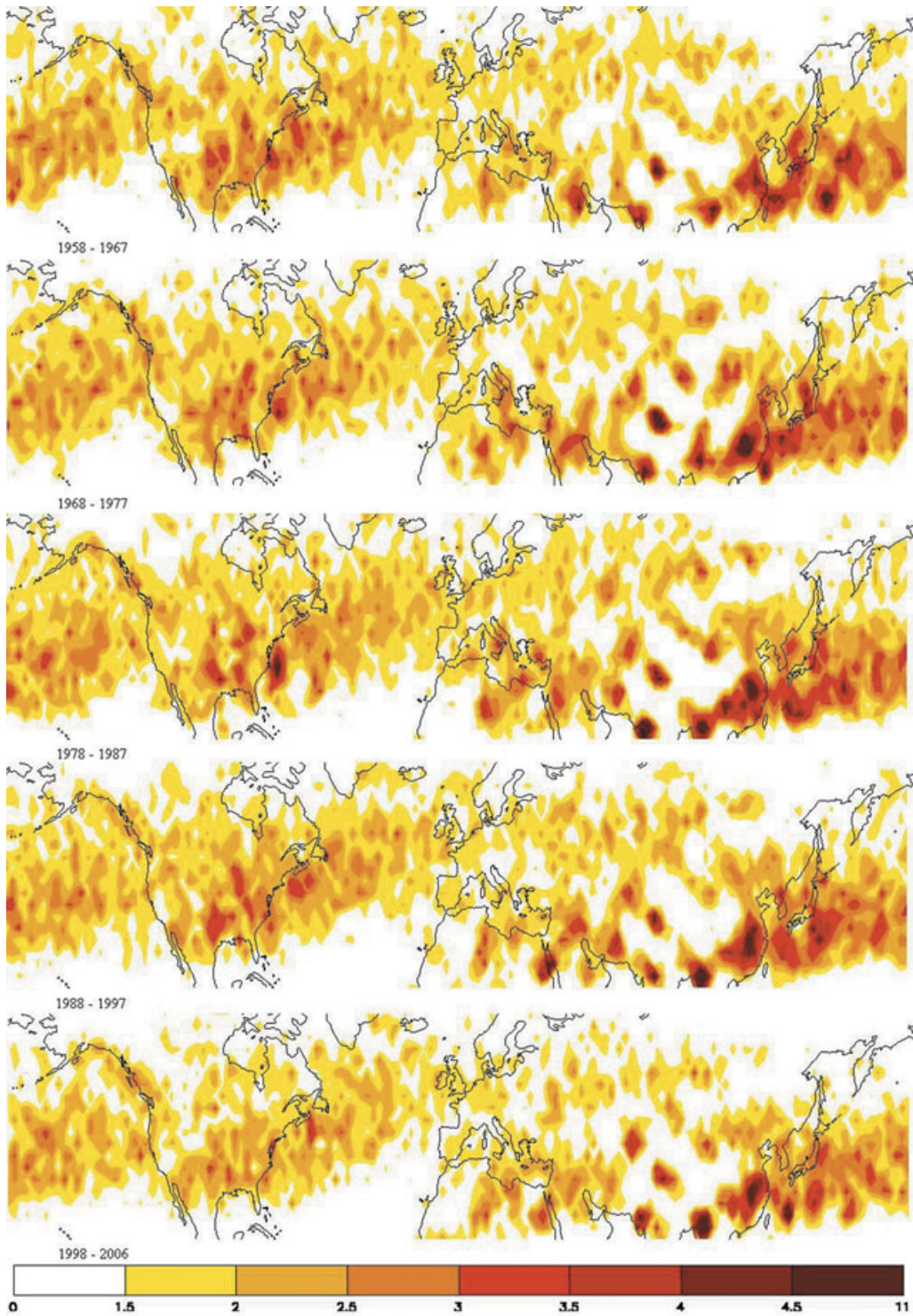


**Figure 6.** Total number of times the vorticity advection at 500 hPa is greater than  $6 \text{ s}^{-2}$  by grid point and year for 1958–1967 (first row), 1968–1977 (second row), 1978–1987 (third row), 1988–1997 (fourth row) and 1998–2006 (fifth row).

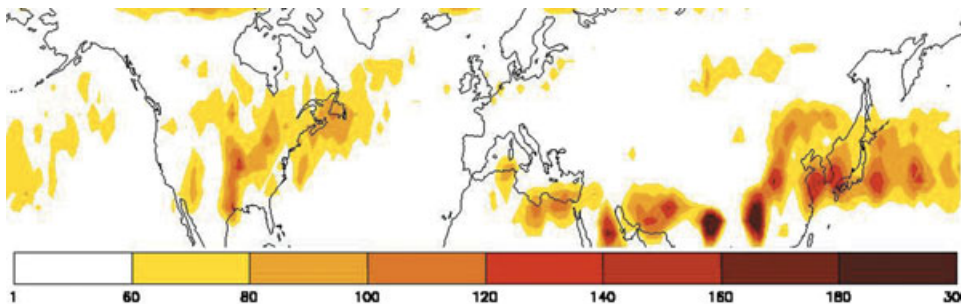


**Figure 7.** Total number of times the difference between the thickness advection at 500–850 hPa and the thickness advection at 200–500 hPa is greater than 150 gpm/s by grid point for 1958–2006 winters (December, January, and February).

avored. The variation of the differential vorticity advection over 10-year intervals (Fig. 10) and of the thickness advection (Fig. 12) shows a redistribution of the maxima within the centers and, in the case of the east coast of North America in Figure 10, a north–south oscillation.

## Discussion and Conclusions

In this section, the results are discussed by region in order to identify the characteristics that contribute to baroclinic development in each location. In Figure 13, a summary of the results found by other authors regarding cyclone tracks, storm tracks, and cyclogenesis regions is shown in order to make the comparison easier.

The Atlantic cyclone track is located north of the storm track and is thus confined to latitudes greater than 50°N. The number of height minima detected in this region increases with time at all levels until the 1998–2006 interval when it decreases. This tendency could be associated with the trends found in the NAO index. There are two distinct maxima at low levels, both trapped between land masses: one over Hudson Bay and another between Greenland and Iceland (associated with the Icelandic low). The first one maintains its intensity throughout the troposphere and is related to the trough over Hudson Bay that appears in the winter climatology of the geopotential height.<sup>38</sup> The advective forcing terms of the omega and geopotential tendency equations have no strong signals

over this zone, which indicates that other processes, such as those related to diabatic heating, ice influence, and orography, are more important for baroclinic development in this region. The maximum between Greenland and Iceland is related more to surface cyclogenesis, its intensity decreasing with height and its arctic fronts signal near the surface. The advection of temperature provides a forcing mechanism that causes upward movement of air masses, but none of the other forcing terms are present, so other processes, such as Greenland orography, are more important.

The Pacific cyclone track is similar to the Atlantic one. Located north of lat 45°N, it extends from the east coast of Asia to the west coast of America with two maxima (also trapped between land masses), one west of Kamchatka and one in the Gulf of Alaska. The first one is associated with high values of TFP and low values of the forcing terms in the omega and geopotential tendency equations. Again, there are other important terms in the development of minima and fronts. The case of the Gulf of Alaska is somewhat different because the vorticity advection plays an important role in the geopotential drops. This indicates that this maximum is influenced by the transient cyclones that originate in the Aleutian low. The cyclones' progress is then impeded by the Rocky Mountains, where they encounter the TFP maxima. In the Pacific basin, a negative trend in the number of height minima is found until the 1998–2006 interval, when it increases.

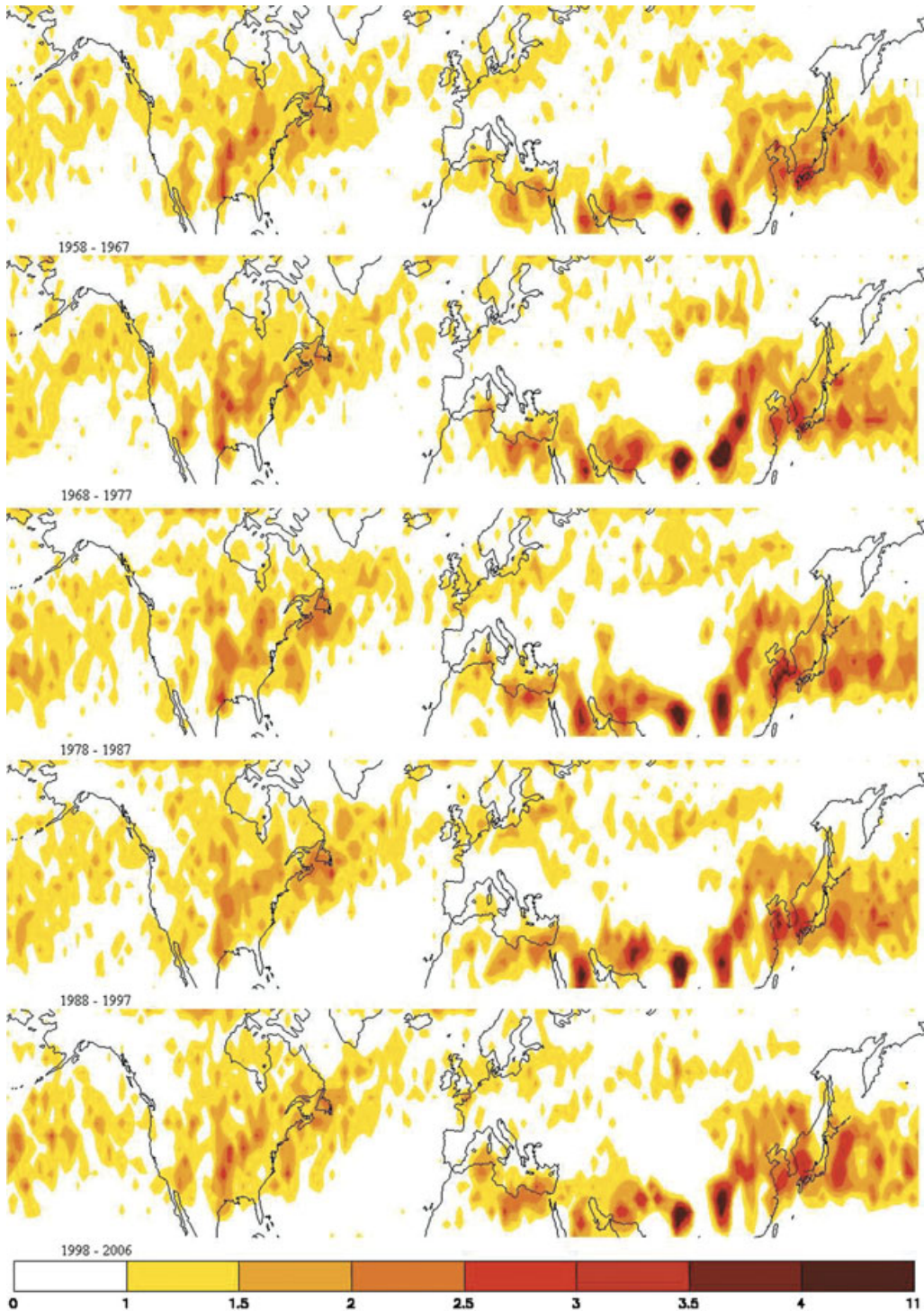


**Figure 8.** Total number of times the difference between the thickness advection at 500–850 hPa and the thickness advection at 200–500 hPa is greater than 150 gpm/s by grid point and year for 1958–1967 (first row), 1968–1977 (second row), 1978–1987 (third row), 1988–1997 (fourth row), and 1998–2006 (fifth row).

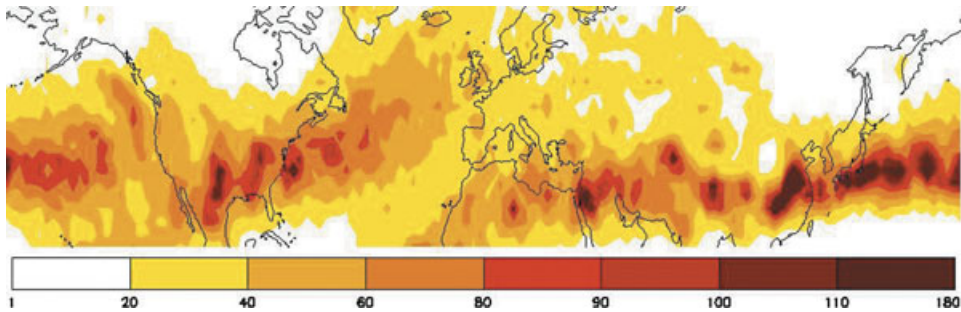


**Figure 9.** Total number of times the difference between the vorticity advection at 200 hPa and the vorticity advection at 850 hPa is greater than  $20 \text{ s}^{-2}$  by grid point for 1958–2006 winters (December, January, and February).

The fact that all the maxima associated with the cyclone tracks are trapped by land masses and the lesser importance of the advective terms in these cases leads us to believe that, when using our method, the effect of stationary lows is of primary importance.

To the south of the cyclone tracks the forcing terms of the omega and geopotential tendency equation mark the regions where the transient cyclones that are associated with the storm track begin to move and deepen. As the movement and deepening of extratropical cyclones slows down when they are more fully developed, these maxima are found near the regions of genesis on the west coasts of the Pacific and Atlantic oceans. The regions of maxima begin on the lee side of the Tibetan Plateau and the Rocky Mountains, respectively. In the case of forcing from the advection of vorticity, these regions extend to the east coast of the oceans, producing strong displacements and upward movements as far as the lysis zones. The height drop from differential advection of temperature usually occurs north of the drop from vorticity advection (i.e., movement of the cyclonic centers). The associated fronts are located over regions of high sea surface temperature where the cold air coming from the continents converges with the warm air over the Gulf and Kuroshio currents. The strong sea surface temperature gradients over the western edge of the Gulf current play a very important role in the development of fronts over the Atlantic.

Orography is a determining factor in the formation of height lows near the earth surface in the Mediterranean region. The maxima are mostly located over the lee side of mountain ranges: the Gulf of Genoa (Alps), Algeria (Atlas Mountains), northeast of the Persian Gulf (Zagros Mountains), west of the Arabian Peninsula (Hijaz and Asir), east of the Black Sea (Greater Caucasus), and east of the Aegean Sea. At higher levels there is a maximum that extends from the western part of the Mediterranean Sea to the northwest of the Canary Islands, resembling the maximum of cut-off lows found by Nieto *et al.*<sup>35</sup> for the European sector. The TFP signal is not very strong over the Mediterranean but it grows in the Middle East, whereas the forcing terms of the omega and geopotential tendency equations are stronger in the south.

In conclusion, the occurrence of height lows as defined in this work appears to be related to the orography near the earth's surface and with surface- and upper-air cyclogenesis in the upper troposphere. Over the cyclone tracks, the surface maxima appear to be trapped by land masses, whereas over the Mediterranean Sea they are located on the lee side of mountain ranges. The forcing terms of the geopotential tendency and omega equations mark the genesis (and, by the vorticity advection terms, the path) of the extratropical cyclones on the storm track. They occur mostly over the western coast of the oceans, beginning and having maxima on the lee side of the Rocky

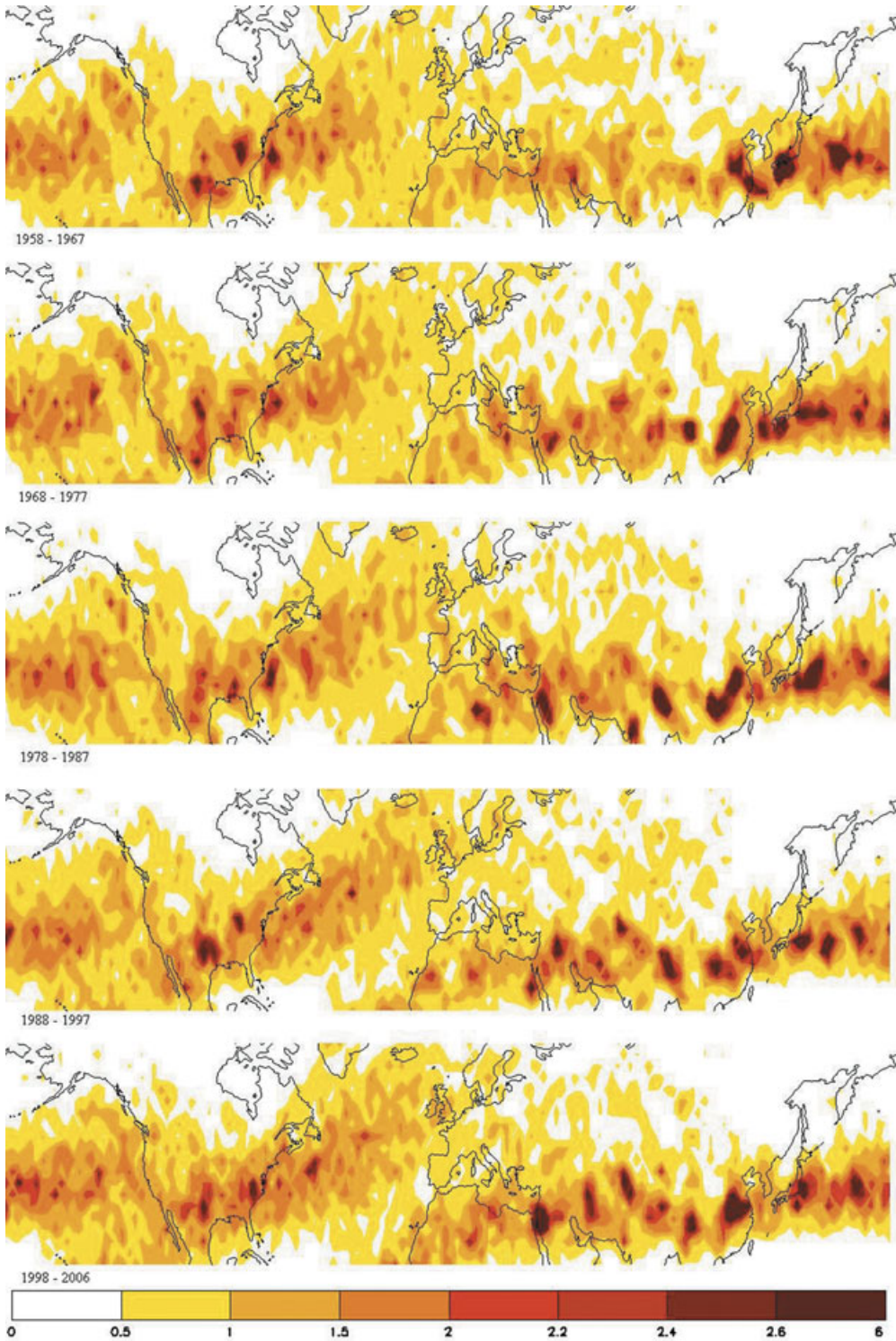


**Figure 10.** Total number of times the difference between the vorticity advection at 200 hPa and the vorticity advection at 850 hPa is greater than  $20 \text{ s}^{-2}$  by grid point and year for 1958–1967 (first row), 1968–1977 (second row), 1978–1987 (third row), 1988–1997 (fourth row), and 1998–2006 (fifth row).

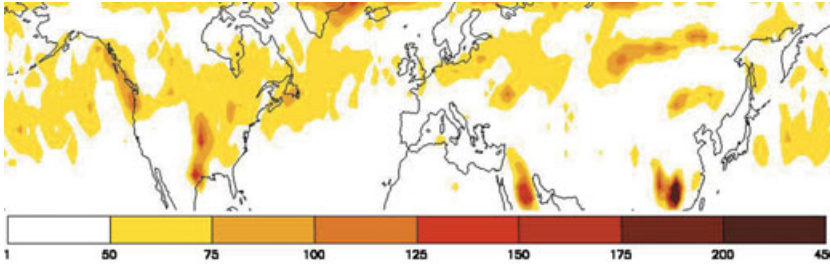


**Figure 11.** Total number of times the thickness advection at 500–850 hPa is greater than 100 gpm/s by grid point for 1958–2006 winters (December, January, and February).

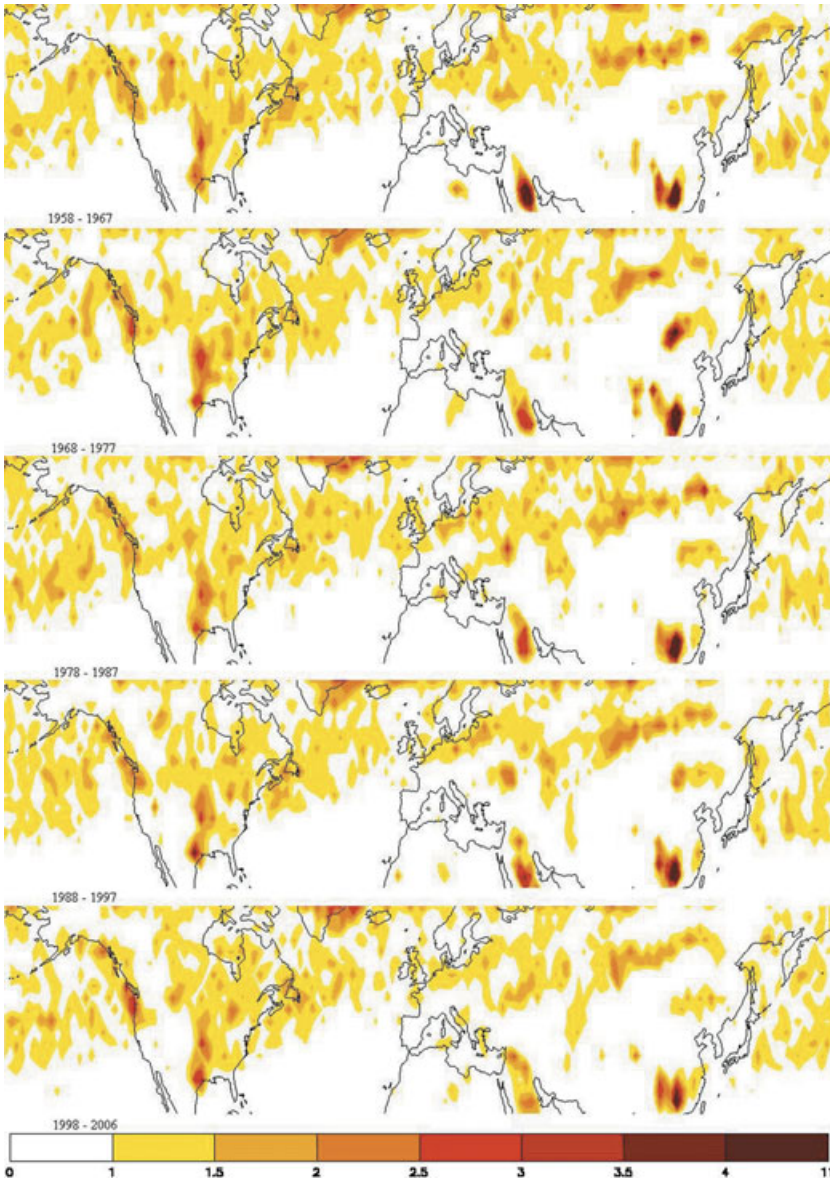


**Figure 12.** Total number of times the thickness advection at 500–850 hPa is greater than 100 gpm/s by grid point and year for 1958–1967 (first row), 1968–1977 (second row), 1978–1987 (third row), 1988–1997 (fourth row), and 1998–2006 (fifth row).

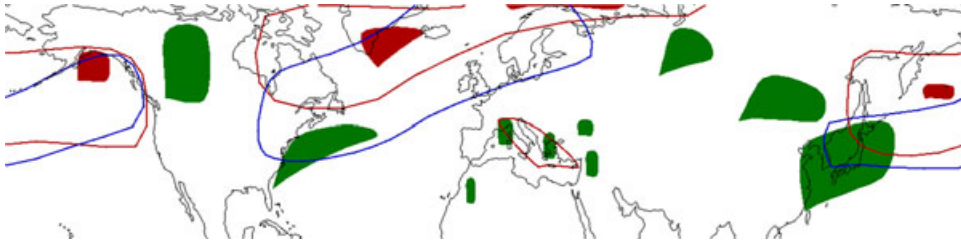


**Figure 13.** Summary of the results of Refs. 9, 4, 19, 14. Red: cyclone tracks found by Wernli and Schwierz<sup>9</sup> (circled) with their maxima (shaded); blue: storm tracks as in Ref. 4; green: cyclogenesis regions as found by Wernli and Schwierz,<sup>9</sup> Trigo *et al.*<sup>14</sup> (Mediterranean region), and Chen *et al.*<sup>19</sup> (East Asia).

Mountains and the Tibetan Plateau. Their associated fronts form from the cold air coming from the continents and converging with the warm air over the Gulf and Kuroshio currents.

There is a high degree of variability over 10-year intervals in all the terms studied. Evident trends are found only for the Atlantic cyclone track (positive) and the Pacific cyclone track (negative) until the last interval, when the tendency reverses. The trend over the Atlantic has been related by other authors to the increase in the NAO index. This increase could also be related to the interdecadal behavior of the TFP center over the Gulf Stream: the stronger circulation of the subtropical high could drag warmer waters into the stream. Over the southern Pacific, the number of fronts is lower during 1978–1997, coinciding with strong ENSO episodes, which means that there are positive anomalies of geopotential height over the region and negative anomalies of precipitation, probably related to this lower number of fronts. In all other cases, it is difficult to detect a specific pattern of temporal variability.

The importance of baroclinic systems on extratropical weather patterns on rainfall, and thus for water resources management, makes it necessary to locate them accurately in numerical models. The climatologies presented here can be used to validate them, comparing the areas and values obtained for each term. This information can be used in model schemes to reproduce the changes associated with different scenarios of climate change and to study the behavior of extratropical cyclones and fronts.

### Conflicts of Interest

The authors declare no conflicts of interest.

### References

- Holton, J.R., J.A. Curry & J.A. Pyle (Eds.). 2003. *Encyclopedia of Atmospheric Sciences*. Academic Press. London. 2780 pp.
- Hurrell, J.W., Y. Kushnir, G. Ottersen & M. Visbeck (Eds.). 2003. The North Atlantic Oscillation climate significance and environmental impacts. *Geophysical Monograph Series*. **134**, 279 pp.
- Enfield, D.B. 1989. El Niño, past and present. *Rev. Geophys.* **27**: 159–187.
- Sickmüller, M., R. Blender & K. Fraedrich. 2000. Observed winter cyclone tracks in the northern hemisphere in re-analysed ECMWF-data. *Quart. J. Roy. Meteor. Soc.* **126**: 591–620.
- Blackmon, M.L., J.M. Wallace, N.C. Lau & S.L. Mullen. 1977. An observational study of the Northern Hemisphere wintertime circulation. *J. Atmos. Sci.* **34**: 1040–1053.
- Wallace, J.M., G. Lim & M.L. Blackmon. 1988. Relationship between cyclone tracks, anticyclone tracks and baroclinic waveguides. *J. Atmos. Sci.* **45**: 439–462.
- Lambert, S.J. 1988. A cyclone climatology of the Canadian Climate Centre general circulation model. *J. Clim.* **1**: 109–115.
- Zhang, X., J.E. Walsh, J. Zhang, *et al.* 2004. Climatology and interannual variability of Arctic cyclone activity: 1948–2002. *J. Clim.* **17**: 2300–2317.
- Wernli, H. & C. Schwierz. 2006. Surface cyclones in the ERA-40 dataset (1958–2001). Part I: novel identification method and global climatology. *J. Atmos. Sci.* **63**: 2486–2507.
- Barry, R.G. & A.M. Carleton. 2001. *Synoptic and Dynamic Climatology*. Routledge. London and New York. 620 pp.
- Serreze, M.C. *et al.* 1993. Interannual variations in snow melt over Arctic sea ice and relationships to atmospheric forcings. *Ann. Glaciol.* **17**: 327–331.

12. Serreze, M.C., F. Carse, R.G. Barry & J.C. Rogers. 1997. Icelandic low cyclone activity: climatological features, linkages with the NAO, and relationships with recent changes in the Northern Hemisphere circulation. *J. Clim.* **10**: 453–464.
13. Gyakum, J.R., J.R. Anderson, R.H. Grumm & E.L. Gruner. 1989. North Pacific cold-season surface cyclone activity: 1975–1983. *Mon. Wea. Rev.* **117**: 1141–1155.
14. Trigo, I.F., T.D. Davies & G.R. Bigg. 1999. Objective climatology of cyclones in the Mediterranean region. *J. Clim.* **12**: 1685–1696.
15. Lambert, S.J. 1996. Intense extratropical Northern Hemisphere winter cyclone events: 1899–1991. *J. Geophys. Res.* **101**: 21319–21325.
16. Schinke, H. 1993. On the occurrence of deep cyclones over Europe and the North Atlantic in the period 1930–1991. *Contrib. Atmos. Phys.* **66**: 223–237.
17. Key, J.R. & A.C.K. Chan. 1999. Multidecadal global and regional trends in 1000mb and 500mb cyclone frequencies. *Geophys. Res. Lett.* **26**: 2053–2056.
18. Graham, N.E. & H.F. Diaz. 1991. Evidence for intensification of north Pacific winter cyclones since 1948. *Bull. Amer. Meteorol. Soc.* **82**: 1869–1893.
19. Chen, S.J., Y.H. Kuo, P.Z. Zhang & Q.F. Bai. 1991. Synoptic climatology of cyclogenesis over East Asia, 1958–1987. *Mon. Wea. Rev.* **119**: 1407–1418.
20. Bjerkness, J. & H. Solberg. 1922. Life cycles of cyclones and the polar front theory of atmospheric circulation. *Geophys. Publ.* **3**: 1–18.
21. Hewson, T.D. 1998. Objective fronts. *Meteorol. Appl.* **5**: 37–65.
22. Mass, C. 1991. Surface synoptic analysis: time for a reassessment? *Bull. Amer. Meteorol. Soc.* **72**: 348–363.
23. Renard, R.J. & L.C. Clarke. 1965. Experiments in numerical objective frontal analysis. *Mon. Wea. Rev.* **93**: 547–556.
24. Kirk, T.H. 1965. A parameter for the objective location of frontal zones. *Meteorol. Mag.* **94**: 351–353.
25. Huber-Pock, F. & C. Kress. 1989. An operational model of objective frontal analysis based on ECMWF products. *Meteorol. Atmos. Phys.* **40**: 170–180.
26. Steinacker, R.A. 1992. Dynamic aspects of frontal analysis. *Meteorol. Atmos. Phys.* **48**: 93–103.
27. Bossart, L.F. 1975. New England coastal frontogenesis. *Quart. J. Roy. Meteor. Soc.* **101**: 957–978.
28. Doyle, J.D. & T.T. Warner. 1993. A numerical investigation of a coastal frontogenesis and mesoscale cyclogenesis during GALE IOP 2. *Mon. Wea. Rev.* **121**: 1048–1077.
29. Alpers, W., J.P. Chen, I.I. Lin & Ch.-Ch. Lien. 2007. Atmospheric fronts along the east coast of Taiwan studied by ERS synthetic aperture radar images. *J. Atmos. Sci.* **64**: 922–937.
30. Iribarne, J.V. & W.L. Godson. 1981. *Atmospheric Thermodynamics*. D. Reidel, Dordrecht. 280 pp.
31. Holton, J.R. 2004. *An introduction to Atmospheric Dynamics*. Academic Press, Burlington, MA. 535 pp.
32. Bluestein, H.B. 1992. *Synoptic–Dynamic Meteorology in Midlatitudes. Vol. I, Principles of Kinematics and Dynamics*. Oxford University Press, New York. 431 pp.
33. Kalnay, E. & Coauthors. 1996. The NCEP/NCAR 40-Year Reanalysis Project. *Bull. Amer. Meteor. Soc.* **77**: 437–471.
34. Hanson, C.J., J. Palutikof & T. Davies. 2004. Objective cyclone climatologies of the North-Atlantic – A comparison between the ECMWF and NCEP Reanalyses. *Clim. Dyn.* **22**: 757–769.
35. Nieto, R., L. Gimeno, L. de la Torre, et al. 2005. Climatologies features of cut-off low systems in the Northern Hemisphere. *J. Clim.* **18**: 3085–3103.
36. Schneiderreit, A., R. Blender, K. Fraedrich & F. Lunkeit. 2005. Icelandic climate and North Atlantic cyclones in ERA-40 reanalyses. *Meteorologische Zeitschrift* **16**: 17–23.
37. Graham, N.E. & H.F. Diaz. 2001. Evidence for Intensification of North Pacific Winter Cyclones since 1948. *Bull. Amer. Meteor. Soc.* **82**: 1869–1893.
38. Peixoto, J.P. & A.H. Oort. 1992. *Physics of Climate*. American Institute of Physics, New York. 520 pp.